RSC Advances

ROYAL SOCIETY OF CHEMISTRY

www.rsc.org/advances

Facile one pot Synthesis and Li-cycling Properties of MnO_2

P. Nithyadharseni[a], M.V. Reddy[a,b*], Ho Fanny[c], S. Adams[b**], B.V.R.Chowdari[a]

[a]Department of Physics, National University of Singapore, Singapore 117542

[b]Department of Materials Science & Engineering, National University of Singapore, Singapore 117546

[c]River Valley High School of Singapore, Singapore 649961

Abstract

For the first time, a molten salt method was attempted to prepare MnO_2 with three different precursors of $Mn(CH_3COO)_2$, $Mn(NO_3)_2$and $MnSO_4{\cdot}H_2O$ by using 0.375MLiNO_3, 0.18MNaNO_3:0.445M KNO_3 as molten salt heated at 380 °C for the application of lithium ion batteries. The prepared compounds were characterized by various techniques such as, X-ray diffraction (XRD), Raman spectroscopy, X-ray photoelectron spectroscopy (XPS), surface area analyzer and scanning electron microscope (SEM), respectively. XRD results revealed the cubic phase of λ-MnO_2 and tetragonal phase of α-MnO_2 and the morphology of the compounds shows spherical particle as well as rod shaped nano-sized particles. The electrochemical performance of the compounds has been evaluated by, galvanostatic cycling (GC), cyclic voltammetry (CV) and electrochemical impedance spectroscopy (EIS). The Li-cycling results indicated that the performance of nano-rod shaped α-MnO_2 prepared by $MnSO_4{\cdot}H_2O$ exhibits stable and high reversible capacity of 845mAh g^{-1}(87.5% capacity retention) at the end of the 50th cycle, cycled at a constant current density of 60 mA g^{-1}, in the potential range of 0.005-3.0 V vs. Li. MnO_2 compound prepared by using three different precursors shows stable coulombic efficiency of 99% after a few cycles.

Keywords: MnO_2; molten salt method; cyclic voltammetry; Anode; Li-ion batteries

Corresponding Authors;*phymvvr@nus.edu.sg; msemvvr@nus.edu.sg; ** mseasn@nus.edu.sg; Telephone number: +65-65162607. Fax: +65-67776126

1. Introduction

Lithium-ion batteries (LIBs) have attracted much attention for various applications such as power portable electronic devices, electric vehicles and sustainable energy generation system due to its high energy density, low memory effect and long cycle life. The first introduced lithium ion battery anode materials was carbon. However, anode materials of carbon and its derivatives of graphene show low specific capacity of 372mAh g^{-1}. Therefore, in order to meet the increasing demand in high energy density and long cycle life lithium ion batteries, a variety of new anode materials have been emerged.

Recently, nanomaterials and transition metal oxides has become the forefront of research to develop the next-generation lithium ion batteries with high power energy density. In order to meet the above requirement, in the past two decades, various nano-sized transition metal oxides (MOs) such as M-Fe, Co, Ni, Cu, Mn, etc., have been extensively studied as anode materials due to its desirable physical and chemical properties, as seen in applications such as catalysis[1-5], biosensors[6], water treatment[7, 8], Li-air batteries [9, 10]and electrochemical super-capacitors[11-25]. Among the above transition metal oxides (TMO), manganese based oxides, such as MnO[26-28], MnO_2[29-32], Mn_3O_4[31], Mn_2O_3[31] and MnO_x[33] have been widely studied as promising anode materials for different applications such as in catalysis and energy storage devices. In addition, manganese oxides (MnO_2) are more superior due to their high theoretical capacity, low cost, environmental compatibility, non-toxicity and natural abundance. For the past two to three decades, MnO_2 and its derivatives are traditionally studied as cathode materials for primary

lithium ion batteries and alkaline batteries[34, 35], but have rarely been reported as an anode material for lithium ion batteries[32, 36, 37]. On the other hand, MnO_2 can exist as numerous crystal structures such as α-MnO_2, β-MnO_2, γ-MnO_2, δ-MnO_2 and λ-MnO_2, etc., of which depends on its nanostructure and morphology as well as fundamental octahedron units of MnO_6. However, MnO_2 shows large volume change during cycling (lithiation-delithiation) processes due to its low electrical conductivity which limits the electronic conductivity, which causes severe electrode pulverization, resulted in poor cycling performance and rate capability. This leads to cracking, and crumbling of the electrode materials. Therefore, in order to solve this problem, many researchers have been proposed on various properties such as structure, design and synthesis of nanostructures as an effective route to accommodate the volume variation.

To prepare MnO_2 nanomaterials with various morphology and physical and chemical properties, various preparation methods such as, sol-gel synthesis[38], wet chemical route[39], hydrothermal techniques[37, 40-44] and precursor technique[45] were used. For example, H. Lai et al., reported MnO_2[46]as anode prepared by facile solution method, which shows stable and lowest capacity of around 300 mAh g^{-1}. Mesoporous γ-MnO_2[47] prepared by template-free self-assembly under ultrasound irradiation exhibits a lowest capacity of 400 mAh g^{-1}. Then, hydrothermal preparation of α-MnO_2[48] shows lowest capacity of 200 mAh g^{-1} even at 30th cycle. Ning Sui et. al., reported that, the preparation of α-MnO_2 and β-MnO_2 with anhydrous manganese sulphate ($MnSO_4$) as a precursor by using molten salts such as KNO_3 and $NaNO_3$, $LiNO_3$ at 380 °C for 3.0 h for the application of large scale preparation and catalytic properties[5, 49]. Very recently Reddy et. al.,[50] prepared MnO_2 compound by molten salt method using 0.5M $LiNO_3$ and 0.5M KNO_3 as molten salt at 310 °C and studied the effect of polymers on structure, morphology and electrochemical properties of MnO_2. For academic interest, we extended the synthesis of MnO_2

oxide by molten salt method at 380 °C for 3.0 h and studied the effect of molten salt (0.375M $LiNO_3$:0.18M $NaNO_3$:0.445M KNO_3) and the influence of different precursors of Mn-salts (Mn-sulphate, Acetate and Nitrate) on structure, morphology on the electrochemical performance.

2. Experimental Procedure

MnO_2 compound was prepared with three different precursors by one pot molten salt method using $LiNO_3$, $NaNO_3$ and KnO_3 as molten salts. The raw materials of all the compounds were purchased from $Mn(CH_3COO)_2$ (Sigma-Aldrich), $Mn(NO_3)_2$ (Alfa-Ultrapure) and $MnSO_4 \cdot H_2O$ (Fluka) and the molten salts of $LiNO_3$ (Merck), $NaNO_3$ (Sigma-Aldrich), and KNO_3 (Merck) were mixed in the molar ratio of (1:10). That is, firstly, Mn Acetate was mixed with $LiNO_3$, $NaNO_3$, and KNO_3 in the molar ratio of 3.75:1.8:4.45 respectively in a crucible. Next, $MnSO_4 \cdot H_2O$ was mixed with $LiNO_3$, NaNO3, and KNO_3 in the molar ratio of 3.75:1.8:4.45 respectively in a crucible. Lastly, $Mn(NO_3)_2$ was mixed with $LiNO_3$, $NaNO_3$, and KNO_3 in the molar ratio of 3.75:1.8:4.45 respectively in a crucible. After thorough mixing, the three mixtures were placed in a box furnace and heated at 380 °C for 3 hours in air at heating rate of 3 °C/min, then allowed to cool at room temperature and were washed with distilled water to remove excess Li-nitrates, hydroxides, or chlorides. The samples were then filtered and dried in the air oven at 80 °C overnight.

The structure and morphology of the compounds were characterized by X-ray diffraction (Bruker, Advance D8) using Cu-Kα radiation source and the results were analysed using Rietveld refinement via TOPAS (v2.1), and the scanning electron microscopy using SEM,-JEOL-JSM 6390), respectively. A Raman spectrum was carried out using a micro Raman spectrometer (Model Lab ram HR Evolution, Horiba Scientific) with an excitation wavelength of 514 nm from an Ar ion LASER, with power of 100 mW. Specific surface area and porosity

information of the samples are obtained by conducting N_2 physisorption experiments at 77 K on Micromeritics ASAP (Tristar 2020, USA) system using Brunauer–Emmett–Teller (BET) and Barrett-Joyner-Halenda (BJH) multipoint methods. The surface chemical compositions of prepared compounds were examined by X-ray photoelectron spectroscopy (XPS) using an AXIS ultra DLD spectrometer (KratosAnalytica). A standard monochromatic AlKa excitation source (1486.6 eV) was employed. The binding energy (BE) scale was calibrated by measuring the reference peak of C1s (BE =284.6 eV). To evaluate the XPS spectra, casa XPS software was used. The electrodes fabrication was carried out by taking active materials of various structured MnO_2 compounds, polyvinylidene fluoride (PVDF) as a polymer binder and Super-P carbon black in 70:15:15 wt. %, respectively and mixing them in N-methylpyrrolidinone (NMP) solvent for overnight. Thus electrode slurry was coated on Cu foil by using Doctor Blade Technique (DBT) and then the foil was cut into circular shape of 16 mm in diameter. The geometrical electrode area was around 2 cm^2 and mass of active material was 2-4 mg. Coin cells were assembled in Argon gas filled glove box (MBraun, Germany) by using the fabricated electrodes as an anode, Li metal (Hohsen Corp., Japan) as counter electrode and 1 M $LiPF_6$ in ethylene carbonate (EC) and dimethyl carbonate (DMC) (1:1 by volume, Merck Selectipur LP40) was used as the electrolyte[51]. The fabricated batteries were electrochemically characterized by cyclic voltammetry (CV) using computer controlled Mac-pile II system (Bio-logic, France) at the scan rate of 0.058 mVs^{-1} in the potential range of 0.005-3.0 V and galvanostatic cycling (GC) using Bitrode battery tester (model SCN, Bitrode, USA), at the current density of 60mA g^{-1}in the potential ranges of 0.005-3.0 respectively. To study the further degradation mechanisms of the MnO_2 electrodes ex-situ XRD was carried out. To recover the cycled composite electrode, the cells were dismantled in the glove box and the electrode was washed in propylene carbonate (PC)

and dried in an oven. The Electrochemical impedance spectroscopy was carried out using Solartron/Gain-phase analyser (model SI 1255) and the plots were recorded by applying 10 mV amplitude over the frequency range from 180 KHz to 3 mHz at room temperature and the data was analysed by using Z-view software (version 2.2, Scribner Assoc., Inc., USA). For clear and better understanding of the compounds name, here onwards, MnO_2 prepared by Mn-acetate, Mn-nitrate and Mn-sulphate were named as M1, M2 and M3, respectively.

3. Results and Discussions

3.1 Structure and morphology

XRD patterns of MnO_2 compounds prepared by molten salt method using three different precursors are shown in Fig. 1 (a) as M1, M2 and M3, respectively. The XRD pattern of M1 can be indexed to cubic phase of λ-MnO_2, which is in very good agreement with JCPDS pattern (# 44-0992-(*a*=8.03Å)) with the space group Fd3m (227). This result well matches with reported literature[52]. But, minor peaks at 21° and 32° (intensity values are <1) are observed, which is the indication of impurities. Whereas, M2 and M3 compounds can be indexed to tetragonal phase of α-MnO_2, which are in very good agreement with JCPDS pattern of (#44-0992) with the space group of 14/m (187). No characteristic peaks related to impurities are observed in M3 compound, which is the indication of pure α-MnO_2 phase obtained by molten salt method using $MnSO_4 \cdot H_2O$ precursor. However, M2 shows some impurities of MnO with minor intensity. The Reitveld refinement XRD pattern of M1 and M3 compound is shown in Fig. 1 (b) and (c). The lattice parameter values observed by TOPAS, for M1 compound is *a* =8.04Å, while the M2 and M3 compounds are close to *a* = 9.86 Å and *c*=2.86 Å, which is in very good agreement with JCPDS pattern. The calculated average crystallite size of the M1, M2 and M3 compounds from Rietveld analysis are 59 nm, 47 nm and 11 nm respectively.

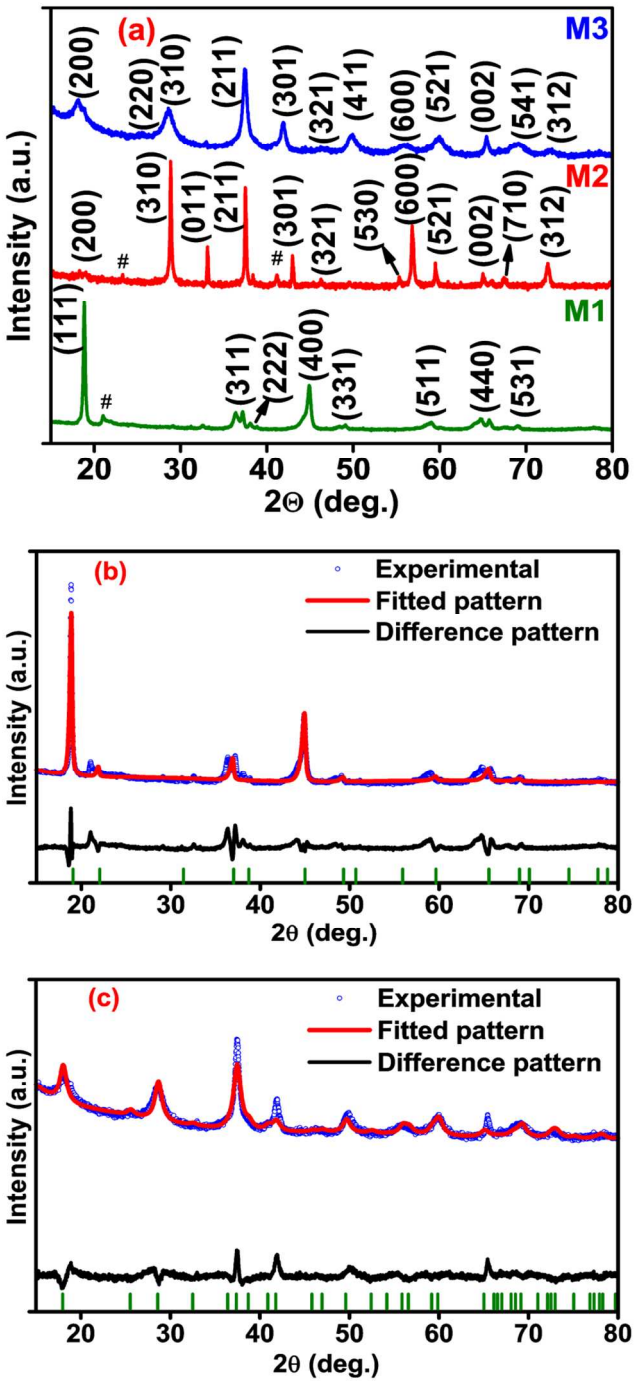

Fig. 1: XRD pattern of MnO_2 compound prepared using three different precursors as M1, M2 and M3 (a), Rietveld XRD spectra of M1 and M3 compounds (b, c)

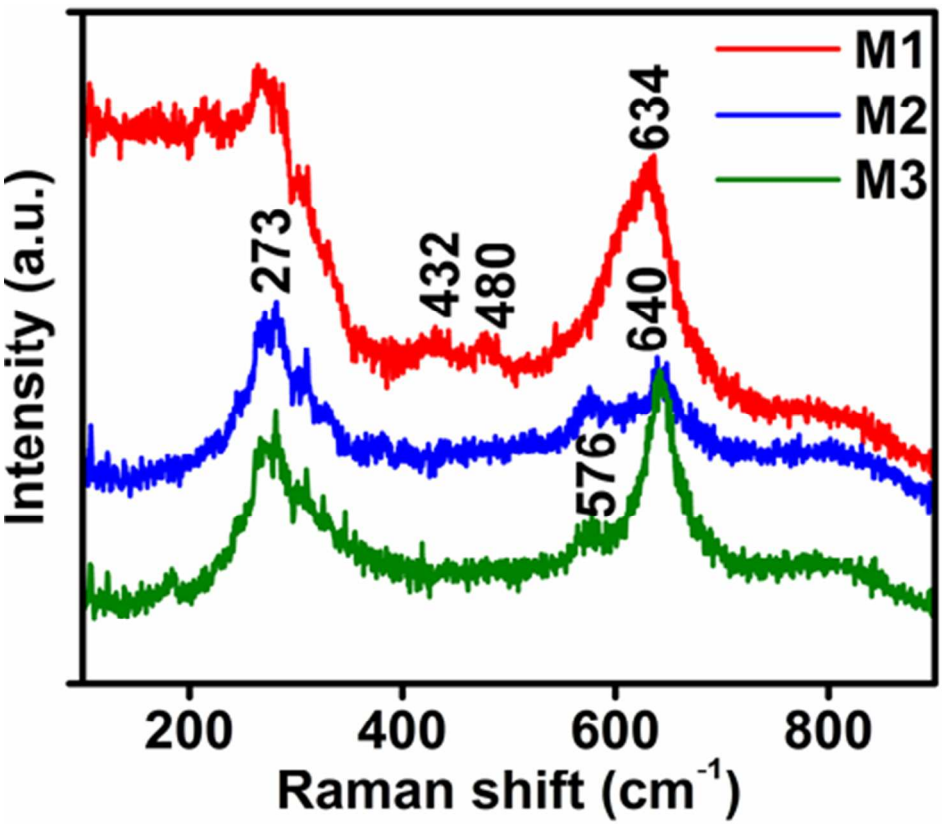

Fig. 2: Raman spectra of MnO_2 as M1, M2 and M3compounds prepared by using three different precursors

To further investigation of structural features of the MnO_2 compound Raman spectroscopy was carried out, as shown in Fig. 2 as M1, M2 and M3 respectively. For all the three compounds, Raman frequencies in the ranges of 500-700 and 200-500 cm^{-1} can be assigned to Mn-O stretching of MnO_6 octahedra and Mn-O-Mn bending vibrations in the MnO_2 octahedral lattice respectively[53]. M1 compound shows four peaks at 634, 480, 432 and 273 cm^{-1}. The M2 and M3 compounds show three peaks at 640, 576 and 273 cm^{-1}. The peak at 576 cm^{-1} in the low wave number region can be attributed to Mn-O stretching vibration which is assigned to A_{1g} symmetry mode while the other strongest peak at 640 cm^{-1} belongs to symmetric stretching vibration of Mn-O of the MnO_6 groups[54-59]. Further studies on chemical composition of the MnO_2 compounds X-ray photoelectron spectroscopy was carried out.

To investigate the chemical composition of the MnO_2 compounds such as M1, M2 and M3, the sample was further characterized by X-ray photoelectron spectroscopy, as shown in Fig. 3 (a-f). Mn 2p spectrum of M1, M2 and M3 compounds are shown in Fig. 3 (a, c, e). The Mn 2p region spectrum consists of two major peaks which are located at 642.8, 654.1 eV for M1, 642.1, 653.7 eV for M2 and 641.9, 653.5 eV for M3 compounds, which can be attributed to $Mn2p_{3/2}$ and $Mn2p_{1/2}$ respectively. The spin-energy separation of M1, M2 and M3 compounds are 11.3, 11.6 and 11.6 eV and these values are in very good agreement with reported literature data[60, 61], indicating 4+ oxidation states of Mn metal. The O 1s spectrum of M1, M2 and M3 compounds are shown in Fig. 3 (b, d, f). For M1 compound, the O 1s spectrum located at 529.5, 531.6 eV, for M2 compound 529.3, 531.8, 533.4 eV and for M3 compound 529.2, 531.8, 533.2 eV. The peaks at 529-530 eV belongs to oxide, 530.5-531.5 eV contributes to hydroxide and 532-533 attributed to water, are in good agreement with reported literature[62].

Compound Name	BET (m^2/g)	Pore volume V_{TOT}, (cm^3/g)	Pore Size (nm)
M1	4.70 (± 0.02)	0.052	12.10
M2	5.10 (± 0.02)	0.051	10.84
M3	38 (± 0.02)	0.254	8.89

Table 1: BET measurements of MnO_2 compound as M1, M2 and M3

The surface area of the MnO_2 compound was measured from BET technique. Fig. 4 (a-c) shows, N_2 adsorption-desorption isotherm of M1, M2 and M3 compounds. The BET surface area, BJH total pore volume and average pore size of the compounds are given in Table 1. The M3 compound shows high BET surface area of 38 m^2/g and Barrett-Joyner- Halenda (BJH) low average pore size of 8.89 nm and high pore volume of 0.254 cm^3/g compared to the other two compounds. These values are much higher than that of others reported in literature prepared by

different method[40]. The isotherms of the compounds are identified as type IV (IUPAC classifications (2-50 nm)), which are characteristics of the mesoporous materials[63]. This prominent enhancement of the M3 (α-MnO_2) compound surface area highlights the overall formation of nanostructured materials through chemical oxidation. The special high BET surface area and mesoporous structure of the rod-shaped MnO_2 provide the possibility of efficient transport of electrons in the Li batteries, which leads to the high electrochemical capacity of the compound.

Fig. 5 (a-c) displays SEM images of M1, M2 and M3 compounds prepared by one-pot molten salt method. The morphology of M1 sample shows high agglomerated nano-sized spherical powder particles with the dimensions of below 100 nm in diameters. Whereas, M2 compound shows the mixing of two different morphologies, that is rod-shaped like structure as well as dendrite form of agglomerated particles, which is in the dimension are close to 100 nm. In contrast, the morphology of M3 compound is found to be of only nanorod-like structure with diameter of below 50 nm.

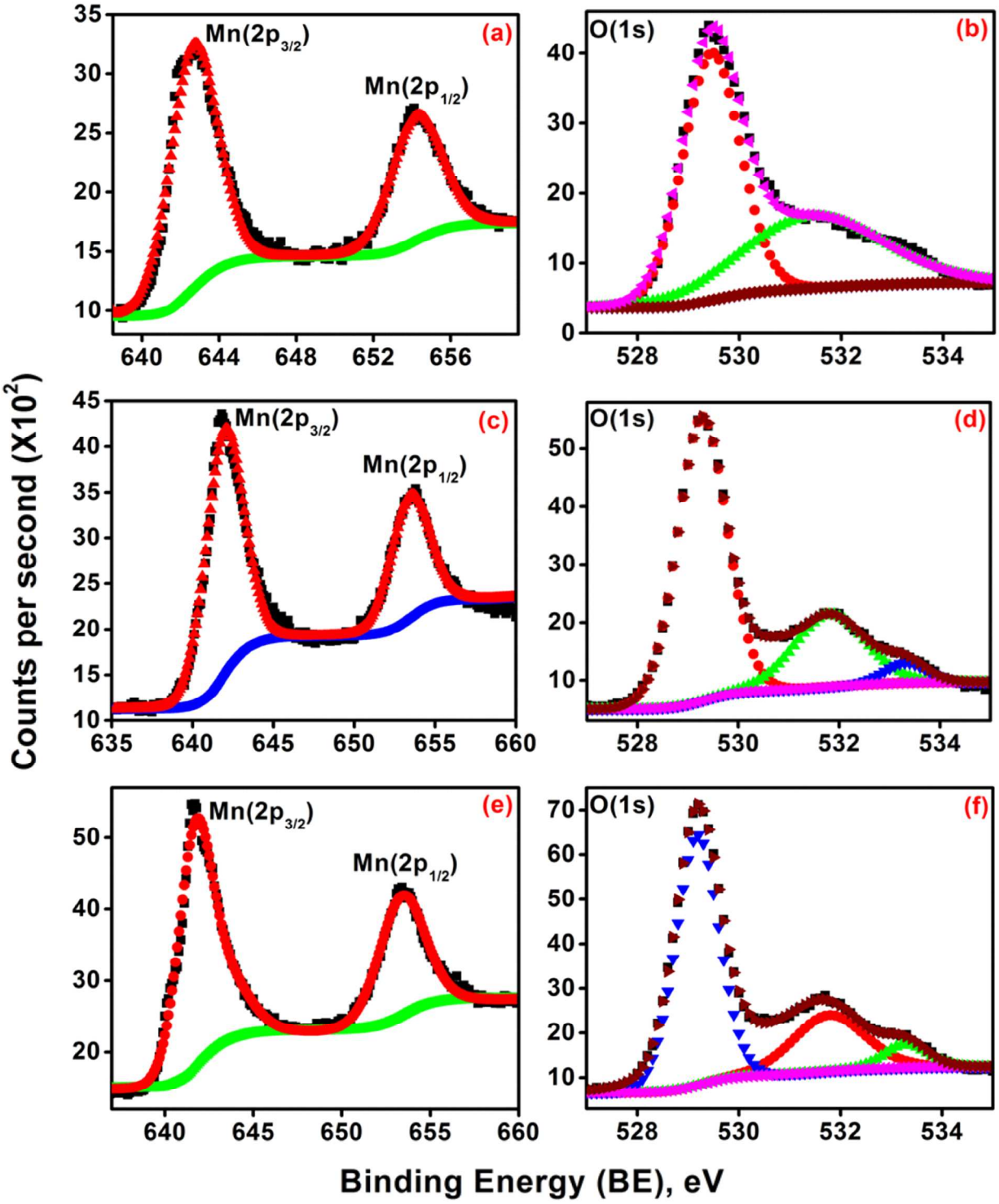

Fig. 3 XPS spectrum of Mn 2p region in $2p_{3/2}$ and $2p_{1/2}$ (a, c, e) and O(1s) region (b, d, f) of M1, M2 and M3 compounds

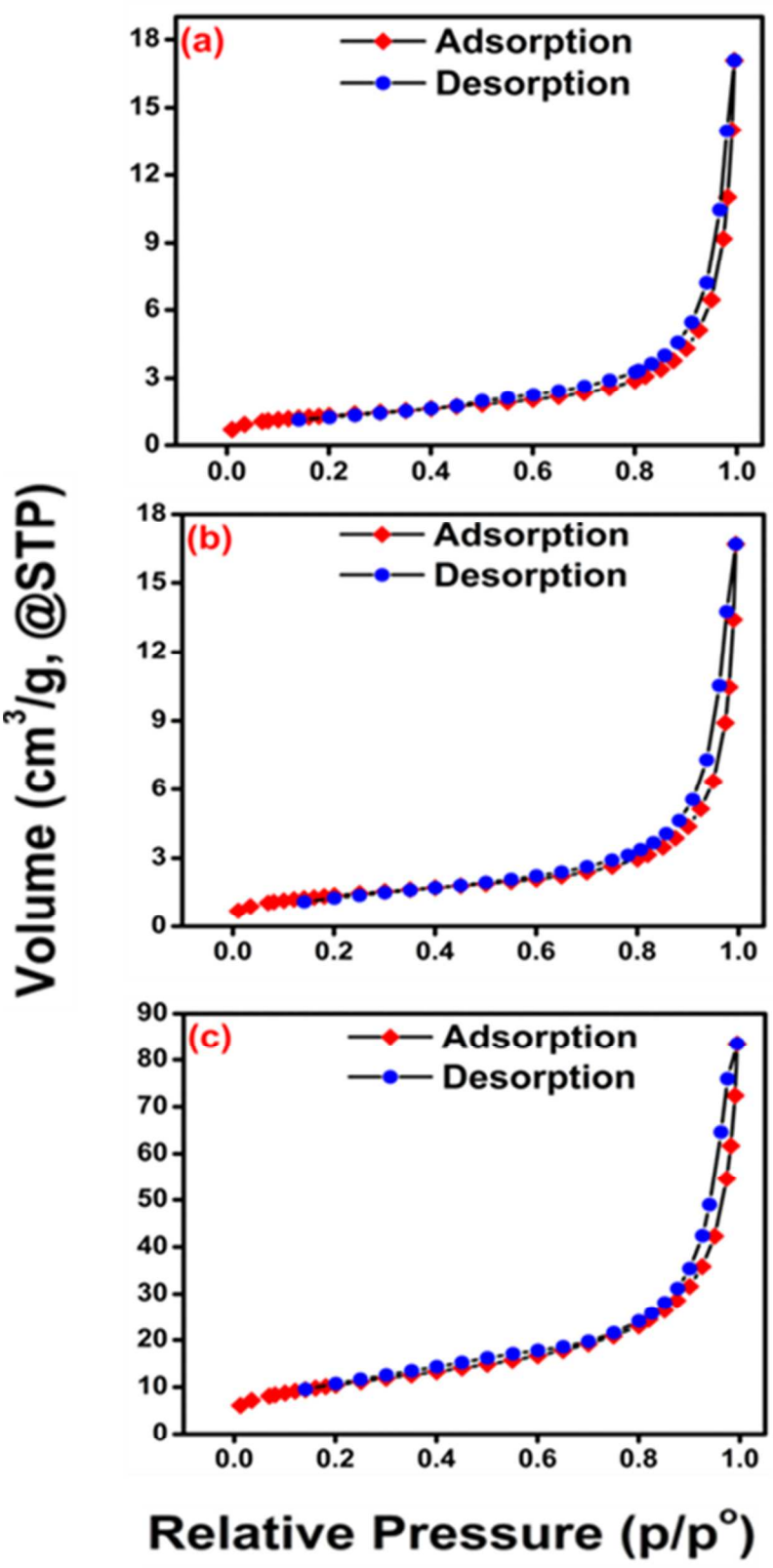

Fig. 4: N_2 adsorption and desorption isotherms of MnO_2 as (a) M1, (b) M2 and (c) M3 compounds

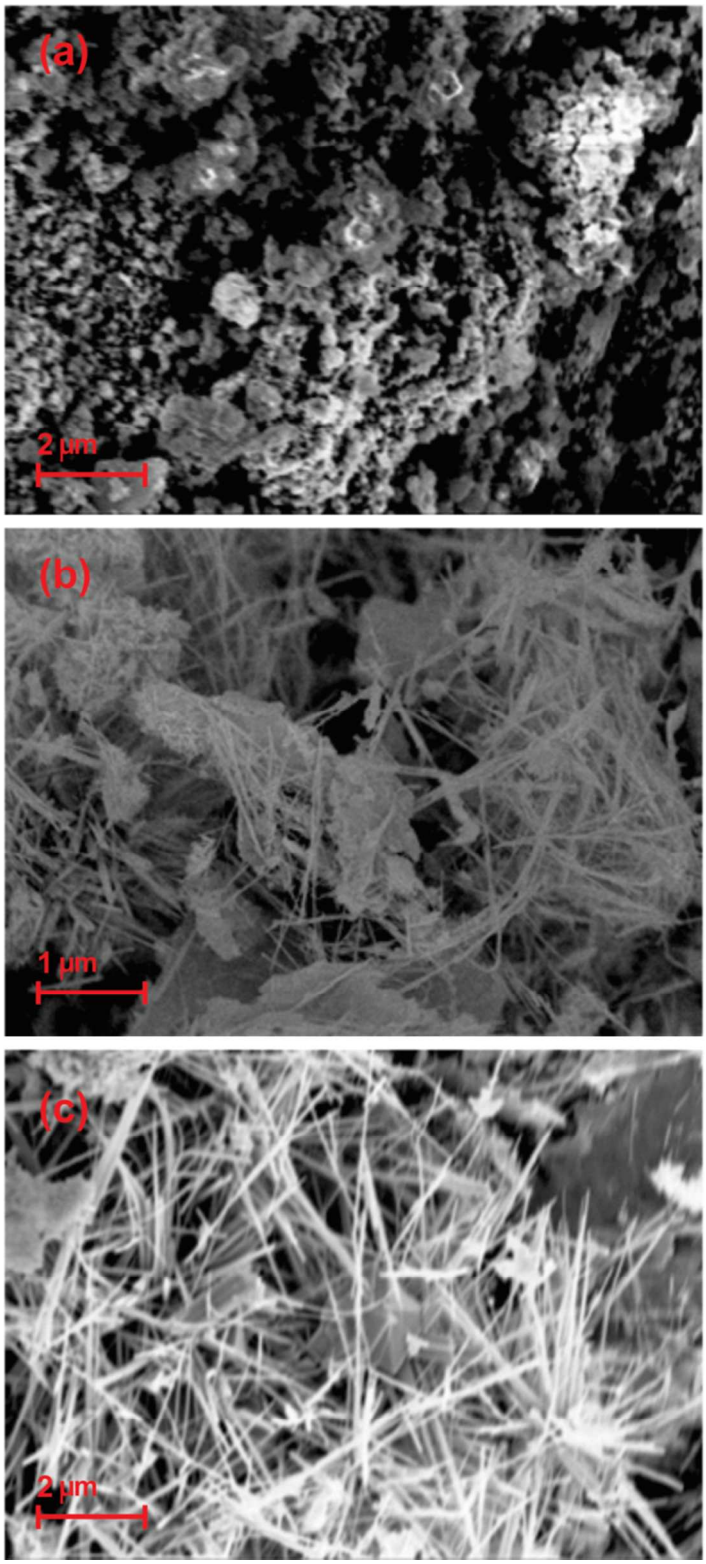

Fig. 5: SEM images of MnO_2 compounds prepared using three different precursors as M1 (a), M2 (b) and M3 (c)

3.2 Electrochemical studies

Galvanostatic cycling of MnO_2 compound prepared by molten salt method using three different precursors are displays in Fig. 6 (a-d) as M1, M2 and M3, respectively. All the compounds were cycled in the range of 0.005-3.0 V vs. Li^+/Li, with the current density of 60 mA g^{-1}. Fig. 6 (a) illustrates that, the first cycle of M1, M2 and M3 compounds. In all the compounds, the first discharge plateau shows two peaks at ~0.75 V and ~0.45 V, which corresponds to electrochemical reaction of MnO_2 with Li and the formation of solid electrolyte interface (SEI) film at the interface of electrode/electrolyte. For the subsequent cycles, the peak at ~0.75 V is vanished and later the peak at ~0.45 V reduced in all the compounds, thus attributed to the confirmation of metallic Mn and Li_2O matrix [64, 65]. In all the compounds the peak ranges from ~0.75 to 0.4 V disappeared in the following cycles, which is ascribed to the SEI formation which only occurs in the first cycle. The other two plateaus can be observed in the first cycle around at 1.3 and 2.3 V, corresponding to electrochemical reduction reaction which is preceded by two steps. On the other hand, the first charge cycle of all the compounds displays two peaks at ~1.0 V and ~1.5 V which corresponds to the oxidation of Mn^0 to Mn^{2+}. In all the transition metal oxides the conversion reaction mechanism has been proposed. Because of the conversion reaction, a large volume expansion is observed, which causes the formation of nanoscaled metal clusters embedded in a Li_2O matrix. Therefore, the electrochemical reaction mechanism of MnO_2 with Li can be expressed as eqn. (1).

$$MnO_2 + 4Li^+ + 4e^- \leftrightarrow 2Li_2O + Mn \quad (1)$$

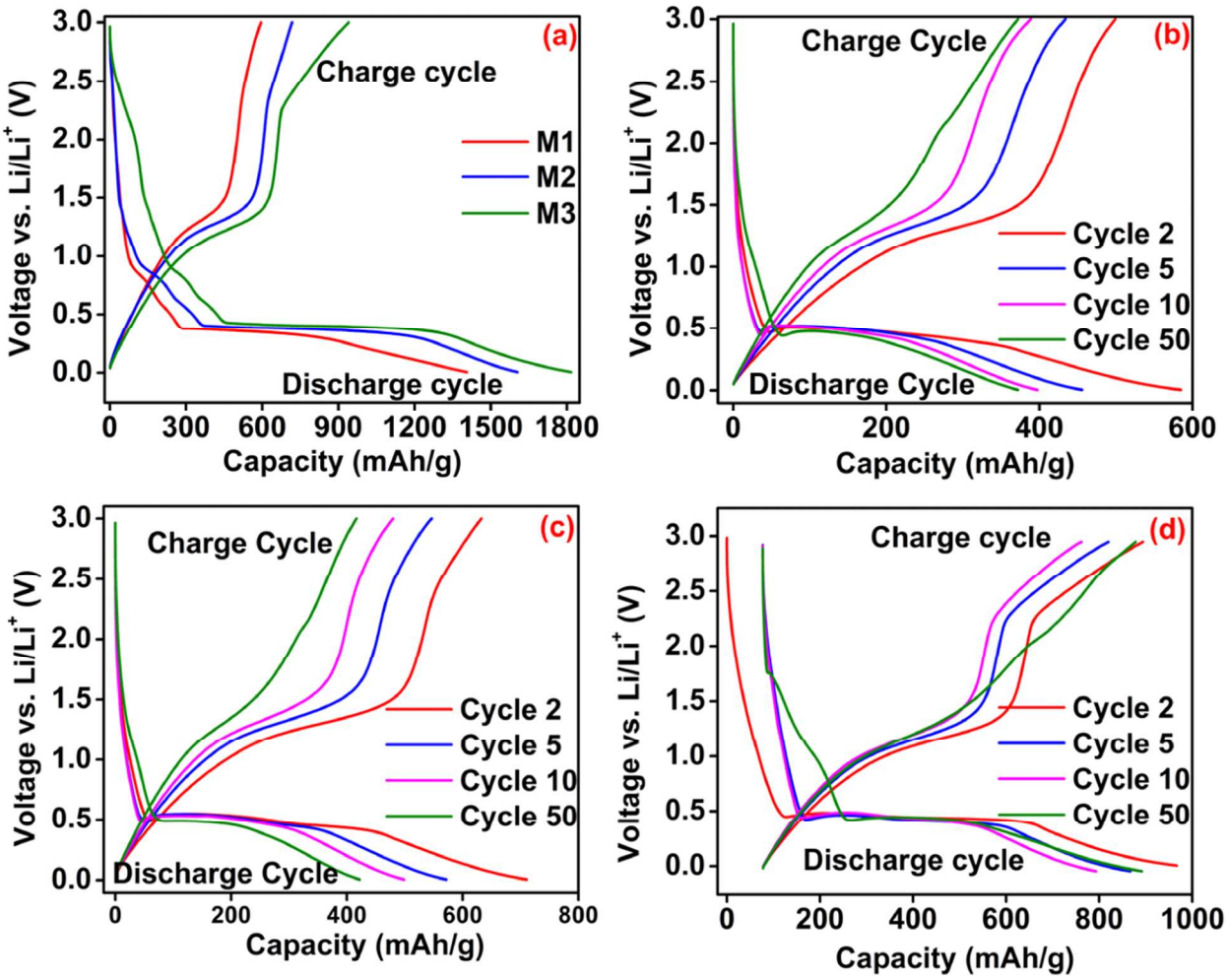

Fig. 6: Galvanostatic cycling plots of MnO_2 for first cycle of all the compounds (a) and selected cycles (2, 5, 10 and 50th cycles) of M1, M2 and M3 compounds (b, c and d)

The first initial discharge and charge capacities of M1, M2 and M3 compounds are, 1406, 1605, 1816 mAh g^{-1} and 595, 717, 940 mAh g^{-1} with initial coulombic efficiencies of approximately 42.3 %, 44.7 %, 51.7 %, respectively. As known, the low coulombic efficiency is serious drawback that impedes the practical applications in the transition metal oxide anode materials. The initial irreversible capacity loss of the M1, M2 and M3 compounds are 822, 888 and 850 mAh g^{-1} respectively. The high initial irreversible capacity loss (ICL) could be attributed to solid electrolyte interface (SEI) film formation which arises from the decomposition of solvent

in the electrolyte. In addition to the formation of the SEI layer, the irreversible capacity for the first cycle is highly dependent on the mobility of Li^+ and e^- during Li extraction process. M3 compound prepared by $MnSO_4 \cdot H_2O$ shows the high capacity and high coloumbic efficiency than other two compounds. Also, the first cycle discharge capacities of all the compounds are larger than the theoretical capacity of MnO_2 compound, which is also be attributed to SEI layer on the electrode surface. The MnO_2 compounds prepared via molten salt method show high initial capacity values than the literature reported by others with different methods[48]. Fig. 6(b-d) shows selected cycles (2^{nd}, 5^{th}, 10^{th} and 50^{th}) of M1, M2 and M3 compounds. In M1 compound, the high charge-discharge capacity fading is observed from the 2^{nd} to 10^{th} cycle, afterwards, it started reducing moderately. But in the M2 compound, high charge-discharge capacity fading is observed from the 2^{nd} to 50^{th} cycle. In contrast, the charge-discharge capacity fading is found to be very low in M3 compound as compared to the other two compounds. The discharge capacity of 50^{th} cycle is almost equal to 3^{nd} cycle of the M3 compound.

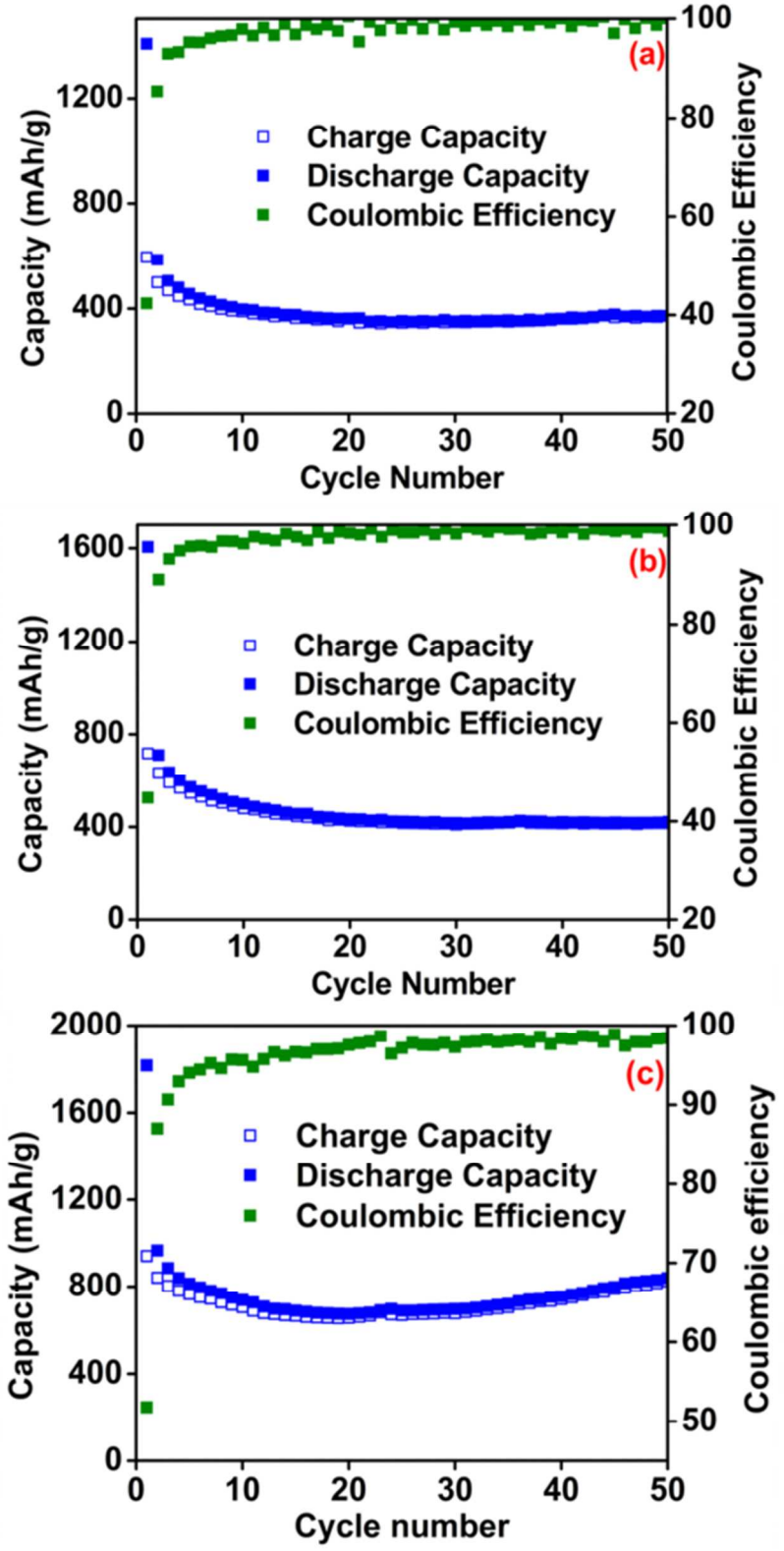

Fig. 7: Cycle number vs. capacity plots of M1 compound (a), M2 compound (b), M3 compound (c) are cycled at 0.005-3.0 V with the current density of 60 mA g^{-1}

Fig. 7 (a-c) illustrates the cyclic performance of M1, M2 and M3 compounds. M1 compound (Fig. 7(a)) shows second cycle capacity of 584 mAh g^{-1} and after that, the capacity values starts to drops down to 361 mAh g^{-1} until 20^{th} cycles. Afterwards, the capacity maintains at this value of 361 mAh g^{-1} until the 40^{th} cycle. Following that, the capacity value slowly rises to 372 mAh g^{-1} at the end of the 50^{th} cycle. M2 compound shows (Fig. 7(b)) a 2^{nd} cycle capacity of 717 mAh g^{-1}, which is then gradually reduced to 499 mAhg^{-1} at 10^{th} cycle. Then, the capacity slowly start to fade down until 40^{th} cycles to 421 mAh g^{-1} and afterwards the same value of 422 mAh g^{-1} is maintained until the 50^{th} cycle. M3 compound (Fig. 7(c)) shows the discharge capacity of 966 mAh g^{-1} for second cycle and slowly drops down to 672 mAh g^{-1} at the end of 20^{th} cycle. Then, the capacity slowly start rise to 695 mAh g^{-1} at the 30^{th} cycle and it slowly increases afterwards and reaches 845 mAh g^{-1} at the end of 50^{th} cycle.

In comparison of all the compounds, MnO_2 prepared by $Mn(CH_3COO)_2$ shows lowest initial capacity of 1405 mAh g^{-1} and also shows low capacity values at the end of 50^{th} cycle, which indicates the low capacity retention of 64%. The low capacity value of the compound could mainly be attributed to its agglomerated spherical particle morphology. Whereas, MnO_2 prepared by $Mn(NO_3)_2$ shows higher initial capacity also higher capacity after 50 cycles (capacity retention of 59%) than M1. The slightly higher capacity might be due to the both spherical particle and nano-rod shaped morphology. In contrast, MnO_2 prepared by $MnSO_4.H_2O$ shows high initial capacity of 1816 mAh g^{-1} also high discharge capacity of 845 mAh g^{-1} (capacity retention of 87.5%) after 50 cycles. The higher capacity could be due to mainly rod shaped morphology of the compound. MnO_2 prepared with precursor $MnSO_4 \cdot H_2O$ by molten salt method also shows higher capacity than the literature reports by others with different methods[44, 46, 48, 60, 63, 66-68].

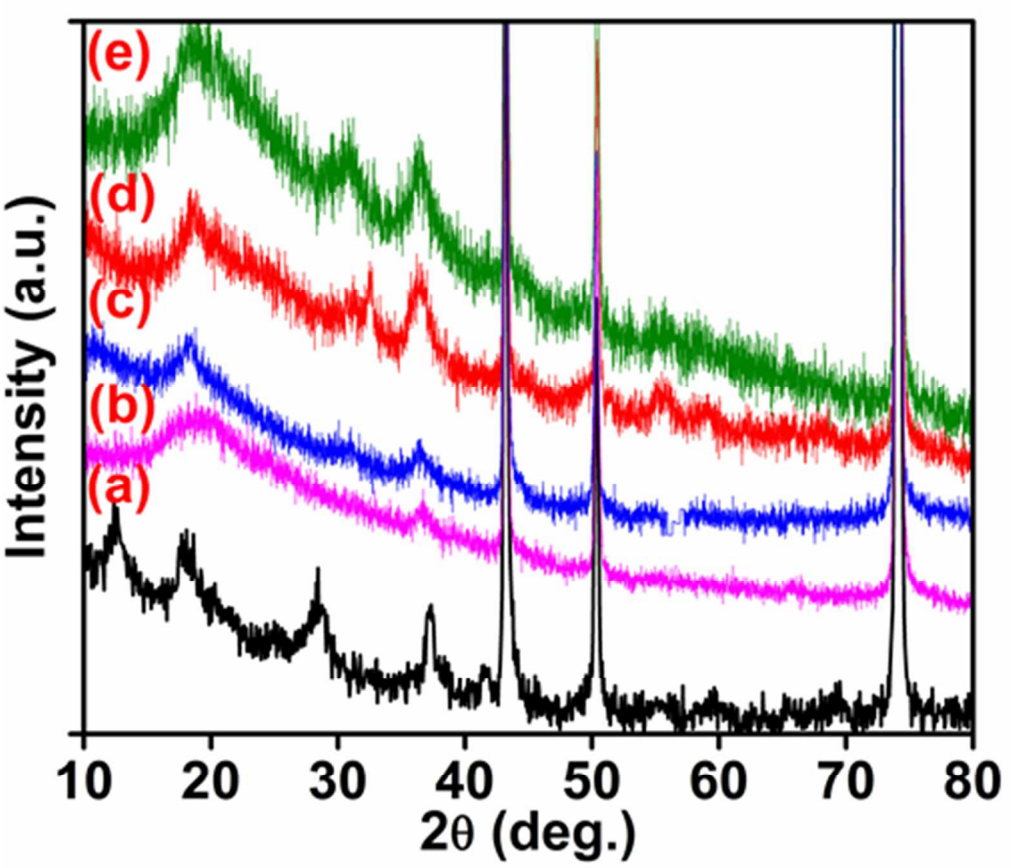

Fig. 8: Ex-situ XRD of MnO_2 (M3) composite electrode (a) and first discharge at 0.005 V (b), 0.5 V (c), 1.0 V (d) and charge at 3.0 V (e) states

To study the further mechanisms of the MnO_2 compound prepared using $MnSO_4 \cdot H_2O$ precursor by molten salt method, Ex-situ XRD of electrodes have been harvested for first cycle at different voltages of discharged at 0.005, 0.5, 1.0 V and charged at 3.0 V, as well as composite electrode, which is shown in Fig. 8 (a-e). XRD pattern of composite electrode and first charge and discharge states at different voltages of MnO_2 (M3) electrodes show three peaks at 43°, 50.5° and 74° which belongs to Cu foil. There is no evidence of impurity peaks such as MnO, Mn_2O_3, MnOOH, Mn_3O_4 and $Mn(OH)_2$, which clearly indicates that the structure of MnO_2 compound remains without any new-phase formation after charge and discharge state[16]. MnO_2 (Fig. 8(a)) composite electrode shows pure phase of MnO_2 compound, which is in very good

agreement with pure XRD shown in Fig. 1. The compound discharged at 0.005 V, shows the amorphous phase structure of MnO_2 which is shown in Fig. 8 (b). However, all the diffraction peaks of the M3 compound discharged at 0.005 V shifted towards to the smaller 2Θ values than the composite electrode. This is an indication that, the inter-planar distance of MnO_2 compound has become larger. XRD spectrum of M3 compound discharged at 0.5 V, 1.0 V and charge at 3.0 V (Fig. 8(c-e)), are similar pattern with that of composite electrode. The diffraction peak positions of the compound charged at 3.0 V is almost similar to the composite electrode, indicating that the inter-planar space of MnO_2 has recovered after de-lithiation of Li^+ [69]. Compared to composite electrode, all the diffraction peaks of the discharged and charged MnO_2 electrodes have become slightly broader, this may be attributed to partially amorphization of the active material during the cycling process.

Cyclic voltammetry (CV) plots of M1, M2 and M3 compounds with few selected cycles (1, 2, 4 and 6) are shown in Fig. 9 (a-c), in the potential range of 0.005-3.0 V, at the scan rate of 0.058 mVs^{-1}, which is used to analyse the kinetic properties of lithium during cycling process in the compound prepared by different precursors. During reduction process in the first cycle, there is a peak in the range from 0.8 to 0.4 V in all the three compounds, which corresponds to the formation of solid electrolyte interface (SEI) film on the electrode surface. The peak range from 0.8 to 0.4 V diminishes in the subsequent cycles, confirming that SEI film formation will take place only in the first cycle. The cathodic peaks at ~0.8 V to 1.5 V and ~0.15 in the first cycle of M1, M2 and M3 compound reveals that the electrochemical reduction process can take place by two steps.

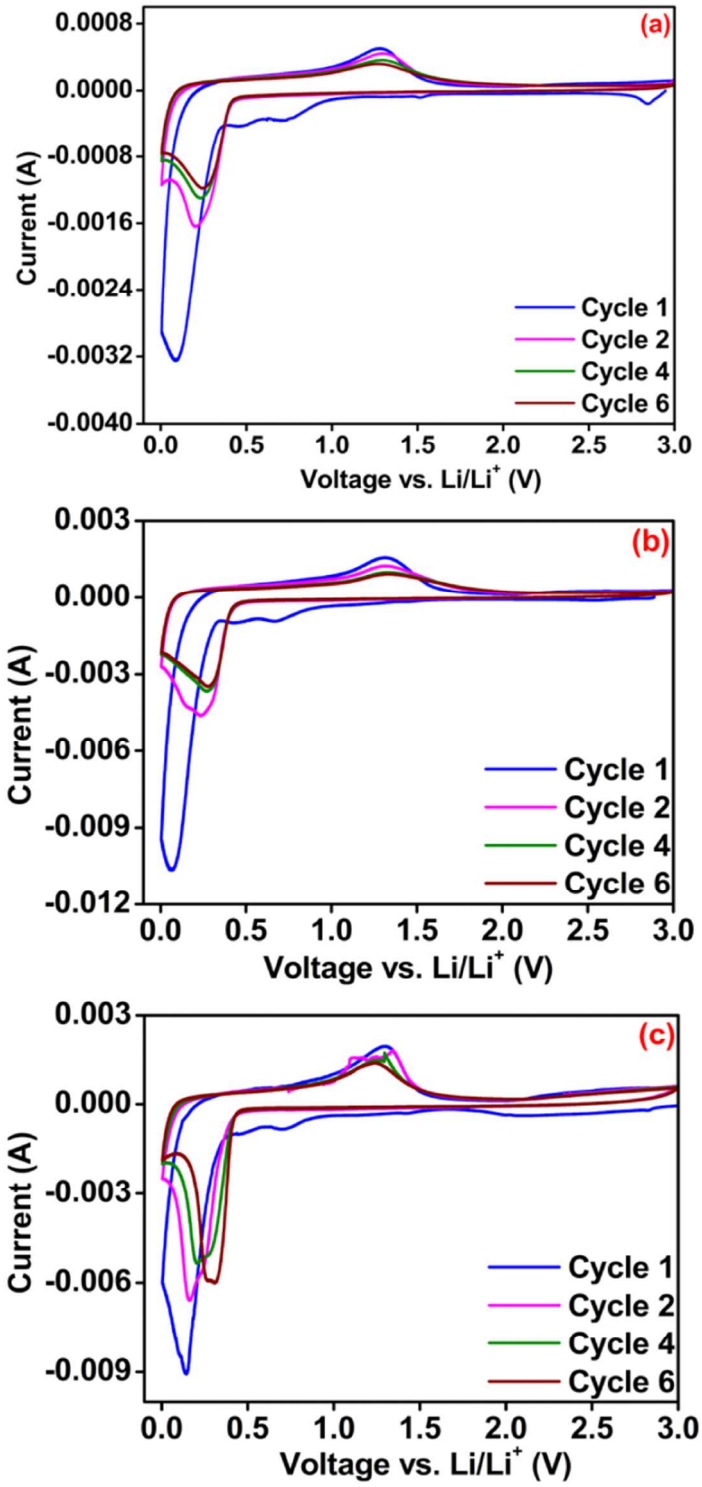

Fig. 9: Cyclic voltammograms of MnO_2 compound prepared by using three different precursors as M1 (a), M2 (b) and M3 (c) cycled in the range of 0.005-3.0 V

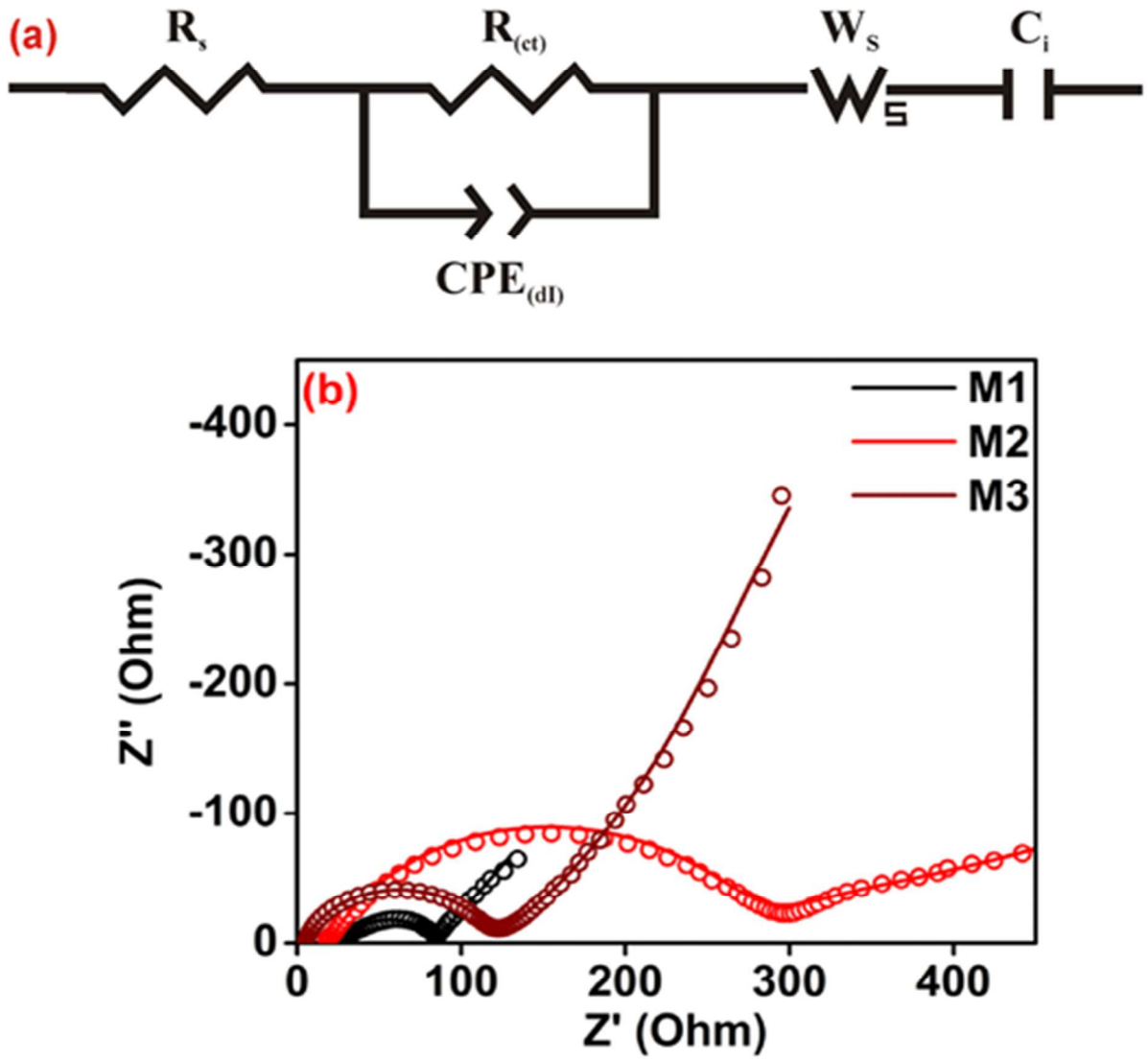

Fig. 10: Equivalent electrical circuit of MnO_2 compounds (a) and Nyquist plots of all (M1, M2 and M3) the compounds for fresh cell (open circuit voltage (OCV))

The first step in the range at ~0.8 V to 1.5 V corresponds to reduction of MnO_2 to Mn^{2+} and the second step at ~0.15 V corresponds to reduction of Mn^{2+} to Mn^0 metal phase, like other transition metals. However, in the subsequent cycles the peak at ~0.8 V to 1.5 V completely disappears but the peak at 0.14 V is shifted to ~0.35 V. The change in shift attributed to the structural reconstruction change induced by the formation of Li_2O and metallic manganese, which is also attributed to the reversible mechanism of MnO_2 as given in Eq. 1. These results are

good accordance with galvanostatic cycling data. The anodic peak is observed at ~1.4 V is to be noted that there is only one step electrochemical oxidation reaction is occurring. During the charging process, Mn can expedite the decomposition of Li_2O as shown in the Eq. 2. Moreover, the anodic and cathodic peak area corresponds to the amount of lithium uptake and removal during cycling process. This peak area is decreasing during subsequent cycles, which is the indication of capacity fading during first few cycles and is in good agreement with GC plots.

$$2Li_2O + Mn \rightarrow MnO_2 + 4Li \quad (2)$$

Further studies on electrochemical behaviours of M1, M2 and M3 compounds, electrochemical impedance spectroscopy was carried out. For all the compounds the data were recorded only for fresh cell (open circuit potential (OCP)). The impedance spectrum of M1, M2 and M3 compounds consists of single semicircle. An intercept at the Z_{real} axis in the high frequency region corresponds to the ohmic electrolyte resistance (R_s). The first semicircle in the high-to-mid frequency region ascribes to the charge transfer resistance (R_{ct}). The inclined line at low frequency region represents the Warburg impedance (Ws), which is associated with lithium-ion diffusion in the active material. The results are plotted as Nyquist plot (Real vs. Imaginary) and are fitted by using an equivalent electrical circuit as shown in Fig. 10 (a). In the entire spectrum of Fig. 10(b), the dotted line represents the experimental data and the straight line corresponds to fitted data. In the equivalent circuit of EIS, apart from the Rs, Rct and Ws the corresponding constant phase element (CPE) is used instead of pure capacitance due to the non-ideal nature of the electrode and also the intercalation capacitance C_i is used. The value of R_s for both M1 and M2 compounds is 15 (±1Ω), while M3 compound has a low value of 4 (±1Ω). The difference in R_s may be due to the difference in the battery package pressure or in the amount of electrolyte added during battery fabrication by manual operation[44]. The charge transfer resistance

values of M1, M2 and M3 compounds are 55, 254 and 112(±1Ω), respectively. The charge transfer resistance of the M1 and M3 compounds are much lower than that of M2 compound. Therefore, the M1 and M3 compounds are more favourable for lithium ion diffusion and transfer with MnO_2 material. These results are very good accordance with galvanostatic cycling and cyclic voltammetry results. The capacitance ($CPE_{(dl)}$) of M1, M2 and M3 compounds are 38, 37, 28 (±3 μF) and the α-values in the range of 0.71-0.78 (±0.01) respectively. The capacitance (C_i) values of M1 and M3 compounds are 2.62 and 0.16 F, respectively.

4. Conclusion

For the first time, MnO_2 compound is prepared by the low temperature molten salt method using three different precursors of $Mn(CH_3COO)_2$, $Mn(NO_3)_2$and $MnSO_4 \cdot H_2O$ with $LiNO_3$, $NaNO_3$ and KNO_3 as molten salts. MnO_2 prepared by $Mn(CH_3COO)_2$ is revealed to be in pure phase of cubic λ-MnO_2 state, while MnO_2 prepared by$Mn(NO_3)_2$ and $MnSO_4 \cdot H_2O$ are in tetragonal phase of α-MnO_2 state. However, M3 compound shows some impurities. XPS spectrum all the compounds show Mn 2p state which is the indication of 4+ oxidation state of Mn metal. SEM images of M1 compound shows agglomerated spherical particles and that of M2 shows mixed morphology of spherical particle in the form of dendrites and rod-shaped nanoparticles. In contrast, SEM images of M3 shows only rod-shaped nano particles. The galvanostatic cycling results of M1 compound shows capacity retention of 64% and M2 compound shows capacity retention of 59% with stable performance. In contrast, M3 compound shows 87.5% of capacity retention with stable and good cycling performance even after 50 cycles.

Acknowledgements

Dr. Nithya gratefully acknowledges NUS for partial financial support through the India research initiative (NUS-IRI-R069000006646) fund. Dr. Reddy and A/Prof. S. Adams would like to thank the National Research Foundation, Prime Minister's Office, Singapore under its Competitive Research Programme (CRP Award No.NRF-CRP 10-2012-6) for research support. Ms. Ho Fanny would like to thank the Gifted Education Branch (GEB), Ministry of Education (MOE) Singapore and River Valley High School for providing her with the opportunity to participate in the Science Research Programme (SRP2014/2015) and the Singapore Science & Engineering Fair (SSEF) 2015.

References

1. Y. Huang, Y. Lin and W. Li, *Electrochimica Acta*, 2013, 99, 161-165.
2. F. W. T. Goh, Z. Liu, X. Ge, Y. Zong, G. Du and T. S. A. Hor, *Electrochimica Acta*, 2013, 114, 598-604.
3. A. Zahoor, M. Christy, H. Jang, K. S. Nahm and Y. S. Lee, *Electrochimica Acta*, 2015, 157, 299-306.
4. H. Zhao, Y. Dong, P. Jiang, G. Wang, J. Zhang, K. Li and C. Feng, *New Journal of Chemistry*, 2014, 38, 1743-1750.
5. N. Sui, Y. Duan, X. Jiao and D. Chen, *The Journal of Physical Chemistry C*, 2009, 113, 8560-8565.
6. W. Zhang, C. Zeng, M. Kong, Y. Pan and Z. Yang, *Sensors and Actuators B: Chemical*, 2012, 162, 292-299.
7. J. B. Fei, Y. Cui, X. H. Yan, W. Qi, Y. Yang, K. W. Wang, Q. He and J. B. Li, *Advanced Materials*, 2008, 20, 452-456.

8. J. Cao, Q. Mao, L. Shi and Y. Qian, *Journal of Materials Chemistry*, 2011, 21, 16210-16215.

9. K. Song, J. Jung, Y.-U. Heo, Y. C. Lee, K. Cho and Y.-M. Kang, *Physical Chemistry Chemical Physics*, 2013, 15, 20075-20079.

10. A. Débart, A. J. Paterson, J. Bao and P. G. Bruce, *Angewandte Chemie*, 2008, 120, 4597-4600.

11. A. Bello, O. O. Fashedemi, M. Fabiane, J. N. Lekitima, K. I. Ozoemena and N. Manyala, *Electrochimica Acta*, 2013, 114, 48-53.

12. X. Zhang, X. Sun, H. Zhang, C. Li and Y. Ma, *Electrochimica Acta*, 2014, 132, 315-322.

13. K. Shimamoto, K. Tadanaga and M. Tatsumisago, *Electrochimica Acta*, 2013, 109, 651-655.

14. A. T. Chidembo, S. H. Aboutalebi, K. Konstantinov, C. J. Jafta, H. K. Liu and K. I. Ozoemena, *RSC Advances*, 2014, 4, 886-892.

15. K. Xiao, J.-W. Li, G.-F. Chen, Z.-Q. Liu, N. Li and Y.-Z. Su, *Electrochimica Acta*, 2014, 149, 341-348.

16. Y. Zhang, C. Yuan, K. Ye, X. Jiang, J. Yin, G. Wang and D. Cao, *Electrochimica Acta*, 2014, 148, 237-243.

17. H. Huang, W. Zhang, Y. Fu and X. Wang, *Electrochimica Acta*, 2015, 152, 480-488.

18. H. Li, X. Zhang, R. Ding, L. Qi and H. Wang, *Electrochimica Acta*, 2013, 108, 497-505.

19. G. Mo, Y. Zhang, W. Zhang and J. Ye, *Electrochimica Acta*, 2013, 113, 373-381.

20. W. Zhou, X. Ma, F. Jiang, D. Zhu, J. Xu, B. Lu and C. Liu, *Electrochimica Acta*, 2014, 138, 270-277.

21. S. Sun, P. Wang, S. Wang, Q. Wu and S. Fang, *Materials Letters*, 2015, 145, 141-144.

22. X. Li, X. Xu, F. Xia, L. Bu, H. Qiu, M. Chen, L. Zhang and J. Gao, *Electrochimica Acta*, 2014, 130, 305-313.

23. J. Chen, C. Jia and Z. Wan, *Electrochimica Acta*, 2014, 121, 49-56.

24. K. Dai, L. Lu, C. Liang, J. Dai, Q. Liu, Y. Zhang, G. Zhu and Z. Liu, *Electrochimica Acta*, 2014, 116, 111-117.

25. S. Deng, D. Sun, C. Wu, H. Wang, J. Liu, Y. Sun and H. Yan, *Electrochimica Acta*, 2013, 111, 707-712.

26. X. Q. Yu, Y. He, J. P. Sun, K. Tang, H. Li, L. Q. Chen and X. J. Huang, *Electrochemistry Communications*, 2009, 11, 791-794.

27. G.-L. Xu, Y.-F. Xu, H. Sun, F. Fu, X.-M. Zheng, L. Huang, J.-T. Li, S.-H. Yang and S.-G. Sun, *Chemical Communications*, 2012, 48, 8502-8504.

28. K. Zhong, X. Xia, B. Zhang, H. Li, Z. Wang and L. Chen, *Journal of Power Sources*, 2010, 195, 3300-3308.

29. B. Choi, S. Lee, C. Fushimi and A. Tsutsumi, *Electrochimica Acta*, 2011, 56, 6696-6701.

30. X. Li, D. Li, Z. Wei, X. Shang and D. He, *Electrochimica Acta*, 2014, 121, 415-420.

31. T. Ahmad, K. V. Ramanujachary, S. E. Lofland and A. K. Ganguli, *Journal of Materials Chemistry*, 2004, 14, 3406-3410.

32. J. Zhao, Z. Tao, J. Liang and J. Chen, *Crystal Growth & Design*, 2008, 8, 2799-2805.

33. D. K. Kim, P. Muralidharan, H.-W. Lee, R. Ruffo, Y. Yang, C. K. Chan, H. Peng, R. A. Huggins and Y. Cui, *Nano Letters*, 2008, 8, 3948-3952.

34. S. Bach, J. P. Pereira-Ramos and P. Willmann, *Electrochimica Acta*, 2011, 56, 10016-10022.

35. F. Tu, T. Wu, S. Liu, G. Jin and C. Pan, *Electrochimica Acta*, 2013, 106, 406-410.

36. J. Li, M. Zou, Y. Zhao, Y. Lin, H. Lai, L. Guan and Z. Huang, *Electrochimica Acta*, 2013, 111, 165-171.

37. J. Chen, Y. Wang, X. He, S. Xu, M. Fang, X. Zhao and Y. Shang, *Electrochimica Acta*, 2014, 142, 152-156.

38. S. Ching, E. J. Welch, S. M. Hughes, A. B. F. Bahadoor and S. L. Suib, *Chemistry of Materials*, 2002, 14, 1292-1299.

39. Y. Oaki and H. Imai, *Angewandte Chemie International Edition*, 2007, 46, 4951-4955.

40. W. Xiao, D. Wang and X. W. Lou, *The Journal of Physical Chemistry C*, 2010, 114, 1694-1700.

41. D. Yan, P. X. Yan, G. H. Yue, J. Z. Liu, J. B. Chang, Q. Yang, D. M. Qu, Z. R. Geng, J. T. Chen, G. A. Zhang and R. F. Zhuo, *Chemical Physics Letters*, 2007, 440, 134-138.

42. X. Wang and Y. Li, *Chemistry – A European Journal*, 2003, 9, 300-306.

43. F. Cheng, J. Zhao, W. Song, C. Li, H. Ma, J. Chen and P. Shen, *Inorganic Chemistry*, 2006, 45, 2038-2044.

44. L. Feng, Z. Xuan, H. Zhao, Y. Bai, J. Guo, C.-w. Su and X. Chen, *Nanoscale Res Lett*, 2014, 9, 1-8.

45. L. Ji and X. Zhang, *Electrochemistry Communications*, 2009, 11, 795-798.

46. H. Lai, J. Li, Z. Chen and Z. Huang, *ACS Applied Materials & Interfaces*, 2012, 4, 2325-2328.

47. Y. S. Yun, J. M. Kim, H. H. Park, J. Lee, Y. S. Huh and H.-J. Jin, *Journal of Power Sources*, 2013, 244, 747-751.

48. Y. Zhang, H. Liu, Z. Zhu, K.-w. Wong, R. Mi, J. Mei and W.-m. Lau, *Electrochimica Acta*, 2013, 108, 465-471.

49. M.-A. Einarsrud and T. Grande, *Chemical Society Reviews*, 2014, 43, 2187-2199.

50. Y. H. L. M.V. Reddy, S. Adams, *Solid State Ionics (abstract accepted in 20th SSI conference)*, 2015.

51. P. Nithyadharseni, M. V. Reddy, B. Nalini, M. Kalpana and B. V. R. Chowdari, *Electrochimica Acta*, 2015, 161, 261-268.

52. W. Ning, C. Xia, L. Guo and S. Yang, *Nanotechnology*, 2007, 18, 475605.

53. A. Ogata, S. Komaba, R. Baddour-Hadjean, J. P. Pereira-Ramos and N. Kumagai, *Electrochimica Acta*, 2008, 53, 3084-3093.

54. W. Chen, Z. Fan, L. Gu, X. Bao and C. Wang, *Chemical Communications*, 2010, 46, 3905-3907.

55. D. Yu, J. Yao, L. Qiu, Y. Wang, X. Zhang, Y. Feng and H. Wang, *Journal of Materials Chemistry A*, 2014, 2, 8465-8471.

56. C. Yang, M. Zhou and Q. Xu, *Physical Chemistry Chemical Physics*, 2013, 15, 19730-19740.

57. H. Xia, Y. Wang, J. Lin and L. Lu, *Nanoscale Res Lett*, 2012, 7, 1-10.

58. C. Julien, M. Massot, R. Baddour-Hadjean, S. Franger, S. Bach and J. P. Pereira-Ramos, *Solid State Ionics*, 2003, 159, 345-356.

59. F. Buciuman, F. Patcas, R. Craciun and D. R. T. Zahn, *Physical Chemistry Chemical Physics*, 1999, 1, 185-190.

60. H. Xia, M. Lai and L. Lu, *Journal of Materials Chemistry*, 2010, 20, 6896-6902.

61. A. L. M. Reddy, M. M. Shaijumon, S. R. Gowda and P. M. Ajayan, *Nano Letters*, 2009, 9, 1002-1006.

62. D. Yan, P. Yan, S. Cheng, J. Chen, R. Zhuo, J. Feng and G. a. Zhang, *Crystal Growth & Design*, 2009, 9, 218-222.

63. B. Li, G. Rong, Y. Xie, L. Huang and C. Feng, *Inorganic Chemistry*, 2006, 45, 6404-6410.

64. B. Sun, Z. Chen, H.-S. Kim, H. Ahn and G. Wang, *Journal of Power Sources*, 2011, 196, 3346-3349.

65. M.-S. Wu, P.-C. J. Chiang, J.-T. Lee and J.-C. Lin, *The Journal of Physical Chemistry B*, 2005, 109, 23279-23284.

66. S. J. Kim, Y. J. Yun, K. W. Kim, C. Chae, S. Jeong, Y. Kang, S.-Y. Choi, S. S. Lee and S. Choi, *ChemSusChem*, 2015, n/a-n/a.

67. J. Fang, Y. F. Yuan, L. K. Wang, H. L. Ni, H. L. Zhu, J. L. Yang, J. S. Gui, Y. B. Chen and S. Y. Guo, *Electrochimica Acta*, 2013, 112, 364-370.

68. Y. Wang, Z. J. Han, S. F. Yu, R. R. Song, H. H. Song, K. Ostrikov and H. Y. Yang, *Carbon*, 2013, 64, 230-236.

69. A. Yuan and Q. Zhang, *Electrochemistry Communications*, 2006, 8, 1173-1178.